Magnetic Detumbling of Fast-tumbling Picosatellites

Conference Paper · October 2018

2 authors:

Robert Fonod
École Polytechnique Fédérale de Lausanne
34 PUBLICATIONS   **320** CITATIONS

Eberhard Gill
Delft University of Technology
347 PUBLICATIONS   **5,557** CITATIONS

Some of the authors of this publication are also working on these related projects:

Project   Distributed Space Systems View project

Project   Optimal Data Fusion for Relative Pose Estimation for Uncooperative Targets View project

IAC-18-C1.3.11

Magnetic Detumbling of Fast-tumbling Picosatellites

Robert Fonod[a]*, Eberhard Gill[a]

[a] *Department of Space Engineering, Delft University of Technology, Kluyverweg 1, Delft, The Netherlands 2629 HS*
* Corresponding Author: r.fonod@tudelft.nl

Abstract

The problem of pure magnetic detumbling of a fast-tumbling picosatellite is considered. A new weighted B-dot control algorithm is proposed. The algorithm enables power reduction while not sacrificing detumbling performance. Analytical expressions relating the maximal expected rotational rate to the minimum sampling time required are presented. Simulation results demonstrate the practical benefits of the proposed approach for picosatellites.

Keywords: Picosatellite, magnetic detumbling, B-dot, attitude control, stability

1. Introduction

The work presented in this paper is motivated by the development of Delfi-PQ satellite [1]. With Delfi-PQ, Delft University of Technology has entered the class of picosatellites and aims at pushing the boundaries of satellite miniaturisation further. This next level of satellite miniaturisation generates new research challenges and offers innovation opportunities. The attitude control and determination subsystem of the Delfi-PQ is an essential cornerstone and is, among others, responsible for the mission-critical detumbling. It is anticipated, that the deployment of Delfi-PQ satellite to low Earth orbit (LEO) will be accomplished by a newly designed, spring-loaded and not in-flight tested, deployment system. Therefore, high initial angular rates up to 180 [deg/s] can be expected. Such high rates will severely impact the communication and power subsystem's functionalities.

In the past decades, a fully magnetic attitude control became a viable and interesting option, especially for low-cost nanosatellites [2–5]. However, developments of fully magnetic control for highly miniaturised picosatellites are still in their infancy. Only recently, preliminary simulation results on successful magnetic detumbling of a slow-tumbling (≤ 6 [deg/s]) picosatellite ($5 \times 5 \times 5$ [cm]) have been reported in [6].

Pure magnetic detumbling of a fast spinning picosatellite creates new challenges, especially due to limited on-board processing and sensing capabilities, magnetorquers saturation, scarce power resources, and inherent underactuation. Driven by these constraints, it is obvious that the detumbling shall be done in a robust and efficient way.

The widely adopted and simple-to-implement B-dot algorithm [7] is, in theory, able to detumble a rotating satellite from any initial angular rate down to approximately twice the orbital rate. However, if the sensing or actuation cycle of the detumbling algorithm is not sufficiently small, the satellite might actually spin up instead of detumbling. Based on Nyquist criterion and rigorous controllability analysis, we provide analytic expressions relating the critical rotational rate of the satellite to the minimum sampling time of the control and sensing loop necessary for successful detumbling.

The B-dot algorithm was recently modified by Avanzini and Giulietti [8] and a reasonable static B-dot gain was derived yielding a quasi-minimum detumbling time. However, for fast tumbling satellites, this B-dot gain needs to be parametrised to efficiently utilise the magnetorquers duty cycle throughout the entire detumbling phase. In this work, we propose a new weighted B-dot control algorithm, where the B-dot gain does not remain constant, but is parametrised by a so-called tumble parameter. This parameter is able to estimate the satellite's absolute tumbling rate using magnetometer readings only. Additionally, the vector version of this parameter is able, in a robust manner, to indicate whether the satellite is detumbled or not. A simple sensor filtering approach is introduced to mitigate the impact of sensor noises and biases caused by on-board electronics. Monte Carlo simulation results are presented to demonstrate the effectiveness of the proposed detumbling algorithm.

Notations: In this paper, bold italic face denotes vectors and matrices; $(\cdot)^T$ stands for transposition; $\mathbb{R}^{n \times m}$ denotes a set of $n \times m$ real matrices, $\mathbb{R}^n$ represents the set of n dimensional real column vectors; $\mathbb{N}$ the set of natural numbers (including $\{0\}$); $\|\cdot\|$ stands for Euclidean vector norm; $|\cdot|$ denotes absolute value; and $\mathcal{N}(\boldsymbol{\mu}, \boldsymbol{\Sigma})$ denotes a density function of a multivariate normal distribution with a mean vector $\boldsymbol{\mu}$ and covariance matrix $\boldsymbol{\Sigma}$.

2. Background

In this section, we will introduce the essential background that allows to study and design a magnetically controlled satellite.

2.1 Coordinate Frames

To represent satellite dynamics, we will use two main reference frames, namely an Earth centred inertial (ECI) reference frame and a satellite body-fixed (body) reference frame.

The origin of the ECI frame is located in the centre of mass (CoM) of the Earth. The z-axis of this reference frame points to the north pole of the ecliptic, the x-axis points towards the vernal equinox (first point of Aries), and the y-axis completes the right-handed orthogonal system. This reference frame will be denoted as $\mathcal{F}_I$.

The origin of the body frame is located in the CoM of the satellite. The axes of this frame coincide with the satellite's principal axes of inertia. Hereafter, the body frame will be denoted as $\mathcal{F}_B$.

2.2 Rotational Dynamics

The rotational dynamics of a rigid body satellite around its CoM are given by Euler's moment equation:

$$\boldsymbol{I}\dot{\boldsymbol{\omega}}_{B/I}^B(t) = -\boldsymbol{\omega}_{B/I}^B(t) \times \boldsymbol{I}\boldsymbol{\omega}_{B/I}^B(t) + \boldsymbol{\tau}_{ext}^B(t), \quad (1)$$

where $\times$ denotes the cross product, $\boldsymbol{\omega}_{B/I}^B \in \mathbb{R}^3$ represents the angular velocity vector of frame $\mathcal{F}_B$ relative to $\mathcal{F}_I$ decomposed in $\mathcal{F}_B$ coordinates, $\boldsymbol{I} \in \mathbb{R}^{3\times3}$ is the inertia matrix, and $\boldsymbol{\tau}_{ext}^B \in \mathbb{R}^3$ is the vector of total external torque acting on the satellite in $\mathcal{F}_B$ coordinates. To avoid extensive notation, the angular velocity vector, $\boldsymbol{\omega}_{B/I}^B$, will be simplified to $\boldsymbol{\omega}^B \triangleq [\omega_x^B \ \omega_y^B \ \omega_z^B]^T$.

The total external torque in (1) can be decomposed as[1]

$$\boldsymbol{\tau}_{ext}^B = \boldsymbol{\tau}_c^B + \boldsymbol{\tau}_d^B, \quad (2)$$

where $\boldsymbol{\tau}_c^B$ is the net disturbance torque and $\boldsymbol{\tau}_d^B$ is the control torque. The net disturbance torque is divided into the following four components:

$$\boldsymbol{\tau}_d^B = \boldsymbol{\tau}_a^B + \boldsymbol{\tau}_s^B + \boldsymbol{\tau}_g^B + \boldsymbol{\tau}_m^B, \quad (3)$$

where

$\boldsymbol{\tau}_a^B$ - is the torque due to residual atmospheric drag,

$\boldsymbol{\tau}_s^B$ - is the torque due to solar and albedo radiation pressure,

$\boldsymbol{\tau}_g^B$ - is the gravity gradient torque due to asymmetric distribution of the mass moment of inertia,

$\boldsymbol{\tau}_m^B$ - is the torque due to residual magnetic dipole and Lorenz forces.

The explicit physical model of the above disturbance torques can be found, for instance, in [9, 10].

2.3 Magnetic Actuation

A magnetic dipole vector $\boldsymbol{m}_c^B \in \mathbb{R}^3$ in $\mathcal{F}_B$, generated by 3 orthogonally mounted electromagnetic coils aligned with the satellite's principal axes of inertia, can be modelled with reasonable accuracy as [11]

$$\boldsymbol{m}_c^B \triangleq \begin{bmatrix} m_{c;x}^B \\ m_{c;y}^B \\ m_{c;z}^B \end{bmatrix} = \begin{bmatrix} N_x A_x i_x \\ N_y A_y i_y \\ N_z A_z i_z \end{bmatrix}, \quad (4)$$

where N_j is the number of windings around the j-th coil, i_j is the current provided in the j-th coil, and A_j is the area of the j-th coil. More accurate magnetic dipole model can be found in [12].

A non-zero magnetic dipole vector (4), generated by satellite body-fixed magnetorquers, will interact with the local magnetic field and generate a control torque vector $\boldsymbol{\tau}_c^B$ according to

$$\boldsymbol{\tau}_c^B = \boldsymbol{m}_c^B \times \boldsymbol{b}_E^B, \quad (5)$$

where $\boldsymbol{b}_E^B \in \mathbb{R}^3$ is the local Earth magnetic field vector expressed in terms of $\mathcal{F}_B$ coordinates.

The torque $\boldsymbol{\tau}_c^B$ can be used, among others, to damp the angular momentum of the satellite close to zero or to de-spin reaction wheels.

2.4 Sensor Model

The local Earth magnetic field $\boldsymbol{b}_E^B$ can be measured on-board the satellite using a triaxial magnetometer sensor. In this paper, for noise filtering purposes and without loss of generality, we assume availability of multiple magnetometers on-board. The model of the i-th magnetometer reading, $\boldsymbol{z}_{raw}^{(i)} \in \mathbb{R}^3$, at discrete time instances $t_k \triangleq kT_s$, $k \in \mathbb{N}$, can be expressed as follows:[2]

$$\boldsymbol{z}_{raw}^{(i)}(t_k) = \left[\boldsymbol{T}_{B/S}^{(i)} \boldsymbol{b}_E^B(t_k) + \boldsymbol{b}_{bias}^{(i)} + \boldsymbol{v}^{(i)}(t_k) \right]_{\mathrm{LSB}}, \quad (6)$$

where $\boldsymbol{v}^{(i)} \in \mathbb{R}^3$ is a random vector satisfying $\boldsymbol{v}^{(i)} \sim \mathcal{N}(\boldsymbol{0}, \boldsymbol{\Sigma}_i)$ and aiming at modelling sensor noise of the i-th magnetometer, $\boldsymbol{b}_{bias}^{(i)} \in \mathbb{R}^3$ is the true static bias of the i-th magnetometer, and $\boldsymbol{T}_{B/S}^{(i)} \in \mathbb{R}^{3\times3}$ is a rotation matrix from $\mathcal{F}_B$ to the i-th sensor frame. Note that $\boldsymbol{T}_{B/S}$ can be also used to account for sensor misalignment and scaling errors. Finally, $[\,\cdot\,]_{\mathrm{LSb}}$ denotes a rounding function driven by the resolution of the magnetometer with respect to the least significant bit (LSB).

---

[1]To further simplify notation, the time-dependency "(t)" of variables will be omitted if there is no ambiguity.

[2]Readings from multiple sensors are assumed to occur simultaneously or with minimum delay. The sampling time T_s will be defined in Section 4.

It is important to note that the above model excludes time-varying biases and assumes magnetorquers being switched off and properly desaturated when taking measurements[3]. The effect of the magnetorquers on the measurements can be easily incorporated into (6) by adding a coupling matrix multiplied by the commanded magnetic dipole moment $\boldsymbol{m}_c^B$ as done in [13].

2.5 Problem Formulation

In this paper, we aim at reducing the angular rate of the satellite from a non-zero initial value $\boldsymbol{\omega}^B(t_0) \triangleq \boldsymbol{\omega}_0^B \neq \boldsymbol{0}$ below a desired absolute angular rate $\omega_{des} > 0$ for all three axes, i.e.,

$$\left| \omega_i^B(t_{det}) \right| \leq \omega_{des}, \quad \forall i \in \{x, y, z\}, \qquad (7)$$

where $t_{det} \geq 0$ denotes the *detumbling time* defined as the time when the condition (7) is satisfied for the first time.

The above aim is to be achieved using a pure magnetic control and feedback provided from the three-axis magnetometers only. The resulting algorithm shall be simple to implement on a low-performance on-board computer and shall take into account physical limitations of the actuators and sensors. The algorithm shall also be able to "assess" the rotational speed of the satellite and shall be able to make efficient use of the magnetorquers (especially at the beginning of the detumbling phase) while not increasing the detumbling time significantly.

Note that, due to physical limitations of the considered setup (pure magnetic actuation and sensing), the satellite's angular rate can be decreased only until it reaches values of approximately twice the orbital rate [14]. Recent research suggests that a rotational rate of about 1.8 of the orbital rate can be achieved around the axis of maximum moment of inertia [15]. To make (7) realistic for all axes, we suggest ω_{des} to be selected such that it satisfies $\omega_{des} \geq 2\omega_o$, where ω_o is the orbital rate.

3. Controller Design and Stability

In this section, we introduce a new weighted B-dot controller and briefly summarise the well-know Lyapunov stability results applied on a rigid-body satellite dynamics actuated by the proposed control law.

3.1 Weighted B-dot Control Algorithm

Many variants of the B-dot controller have been presented in the literature. The simplest one is given by a static linear feedback of the form [7]

$$\boldsymbol{m}_d^B = -k_{\dot{b}}^c \, \dot{\boldsymbol{b}}_E^B, \qquad (8)$$

where $k_{\dot{b}}^c > 0$ is the constant controller gain, $\dot{\boldsymbol{b}}_E^B$ is the time derivative of $\boldsymbol{b}_E^B$ (hence the name B-dot), and $\boldsymbol{m}_d^B$

is the desired dipole moment to be generated by the magnetorquers. In an ideal case $\boldsymbol{m}_c^B = \boldsymbol{m}_d^B$. In practice, however, the commanded dipole moment might be different from the desired one. This is due to magnetorquers' physical limitations (e.g., saturation) which need to be addressed. Control efficiency of the B-dot controller improves as the orbit inclination angle increases [16].

Although (8) is simple to implement [17], the choice of the control gain $k_{\dot{b}}^c$ is not straightforward. A high value may lead to frequent saturation of the magnetorquers, whereas a low value might lead to an inefficient use of the magnetorquers and very long detumbling time t_{det}. Additionally, a static gain is not a good practical solution for both, very high and at the same time low angular rates, as the desired dipole moment is proportional to the absolute change of the magnetic field, i.e., $\|\boldsymbol{m}_d^B\| \propto \|\dot{\boldsymbol{b}}_E^B\|$, which directly relates to the angular rate of the satellite.

In this paper, we adopt the structure of the modified B-dot controller proposed by Avanzini and Giulietti [8], where the desired dipole moment is computed as

$$\boldsymbol{m}_d^B = -\frac{k_{\dot{b}}(p)}{\|\boldsymbol{b}_E^B\|} \dot{\hat{\boldsymbol{b}}}_E^B, \qquad (9)$$

where $\dot{\hat{\boldsymbol{b}}}_E^B$ is the time derivative of the unit vector $\hat{\boldsymbol{b}}_E^B = \boldsymbol{b}_E^B / \|\boldsymbol{b}_E^B\|$. This unit vector is parallel to the Earth's magnetic field vector $\boldsymbol{b}_E^B$, expressed in $\mathcal{F}_B$. In practice, the time derivative of $\hat{\boldsymbol{b}}_E^B$ is difficult to measure directly. However, as will be shown in the next section, $\dot{\hat{\boldsymbol{b}}}_E^B$ can be estimated by differentiating the magnetic field vector obtained from the body-mounted magnetometers.

In (9), instead of using a static control gain as in [8], we parametrised the control gain by p, the so called *tumble parameter*, as follows

$$k_{\dot{b}}(p) = \frac{k_{\dot{b}}^*}{\varphi p + \varepsilon}, \qquad 0 \leq p \leq 1, \qquad (10)$$

where $0 \leq \varphi < \infty$ is the rate factor, $0 < \varepsilon \leq 1$ is the tuning parameter, and $k_{\dot{b}}^*$ is the sub-optimal static gain derived in [8] as

$$k_{\dot{b}}^* = 2\omega_o \left(1 + \sin(\xi)\right) I_{min}, \qquad (11)$$

where ω_0 is the orbital rate (mean motion), ξ is the inclination of the orbit plane relative to the geomagnetic equator and I_{min} is the minimum mass moment of inertia of the satellite. It is obvious that for $\varphi = 0$ and $\varepsilon = 1$, (9) becomes equivalent with the modified B-dot law of Avanzini and Giulietti [8]. A pure static gain $k_{\dot{b}}(p) = k_{\dot{b}}^*$ results in a quasi-minimum detumbling time [8].

---

[3]This assumption arises from the fact that we limit the magnetorquers duty cycle and allow extra time for the magnetorquers to desaturate, see the discussion in Section 4.

The tumble parameter p represents the satellite's absolute sensable angular rate and can be related to the satellite angular velocity as (if $|\omega_i^B| \le |\omega_{max}|, \forall i \in \{x, y, z\}$)

$$p \approx \frac{\|\boldsymbol{\omega}^B\|}{\sqrt{3}|\omega_{max}|}, \qquad (12)$$

where ω_{max} is the maximal absolute rotational rate of the satellite that the on-board magnetic sensor suite is able to sense without aliasing effects, see the discussion on ω_{max} in Section 4. The on-board computation of p using magnetometer data will be detailed in the next section.

Note that the sign of the desired moment (9), on a per-axis basis, is opposite to the rate of change of the magnetic field along the respective axis and its magnitude is inversely proportional to the tumbling parameter p. The motivation behind this design choice is to reduce the power consumption of the magnetorquers, especially during the early stages of the detumbling mode (most critical phase), while not sacrificing the detumbling performance measured by t_{det}. As will be shown later, by proper choice of ε, the variable control gain $k_{\dot{b}}(p)$ can be tuned to approach the sub-optimal gain $k_{\dot{b}}^*$ as the detumbling phase approaches its end ($t \to t_{det}$).

Remark 1. *Similarly as the classical B-dot controller given in* (8), *the weighted B-dot controller* (9) *does not require any knowledge of the inertia* $\boldsymbol{I}$ *and is able to detumble the satellite to approximately twice the orbital rate.*

3.2 Stability Sketch of the Weighted B-dot Controller

We will neglect the disturbance torques (3) from the following analysis as their influence during the detumbling phase is usually very minor. Hence, for $\boldsymbol{\tau}_d^B = \boldsymbol{0}$, the equation of motion (1) simplifies to

$$\boldsymbol{I}\dot{\boldsymbol{\omega}}^B = -\boldsymbol{\omega}^B \times \boldsymbol{I}\boldsymbol{\omega}^B + \boldsymbol{\tau}_c^B. \qquad (13)$$

From a Lyapunov stability perspective, the aim is to drive $\boldsymbol{\omega}^B \to \boldsymbol{0}$ as $t \to \infty$ for any $\boldsymbol{\omega}_0^B \neq \boldsymbol{0}$ (asymptotic stability). To proceed, we define a positive definite Lyapunov function candidate as

$$V(\boldsymbol{\omega}^B) = \frac{1}{2}(\boldsymbol{\omega}^B)^T \boldsymbol{I}\boldsymbol{\omega}^B, \qquad (14)$$

where the right hand side of (14) represents the true kinetic energy over the rigid body. Note that the inertia matrix $\boldsymbol{I}$ is symmetric positive definite and has positive eigenvalues called principal moments of inertia [9].

To apply the 2-nd theorem of Lyapunov, we take the time-derivative $^B\mathrm{d}/\mathrm{d}t(\cdot)$ of the kinetic energy (14) as (note that $\boldsymbol{I}$ is constant in $\mathcal{F}_B$ and the right hand side of the Lyapunov function is frame-independent)

$$\begin{aligned} \dot{V}(\boldsymbol{\omega}^B) &= \frac{1}{2}\left((\dot{\boldsymbol{\omega}}^B)^T \boldsymbol{I}\boldsymbol{\omega}^B + (\boldsymbol{\omega}^B)^T \boldsymbol{I}\dot{\boldsymbol{\omega}}^B\right) \\ &= (\boldsymbol{\omega}^B)^T \left(-\boldsymbol{\omega}^B \times \boldsymbol{I}\boldsymbol{\omega}^B + \boldsymbol{\tau}_c^B\right) \\ &= (\boldsymbol{\omega}^B)^T \boldsymbol{\tau}_c^B. \end{aligned} \qquad (15)$$

It is obvious from (15) that, if $\boldsymbol{\tau}_d^B = \boldsymbol{0}$, the change of kinetic energy is due to the control torque only and it decreases only if the dot product of the angular velocity and control torque is negative, i.e., $(\boldsymbol{\omega}^B)^T \boldsymbol{\tau}_c^B < 0$.

Using the basic theorem of kinematics, we have

$$\dot{\hat{\boldsymbol{b}}}_E^B = \frac{^B\mathrm{d}}{\mathrm{d}t}\left(\boldsymbol{T}_{I/B}\hat{\boldsymbol{b}}_E^I\right) = \boldsymbol{T}_{I/B}\dot{\hat{\boldsymbol{b}}}_E^I - \boldsymbol{\omega}^B \times \hat{\boldsymbol{b}}_E^B, \quad (16)$$

where $\boldsymbol{T}_{I/B}$ is a transformation matrix from $\mathcal{F}_I$ to $\mathcal{F}_B$. Since $\dot{\hat{\boldsymbol{b}}}_E^I$ varies at most at angular rate of approximately $2\omega_o$, for high angular rates $\boldsymbol{\omega}^B$, the rate of change of the magnetic field in the body frame is mainly due to the rotation of the satellite. Hence, for $\|\boldsymbol{\omega}^B\| \gg 2\omega_o$, the right hand side of (16) can be approximated as

$$\dot{\hat{\boldsymbol{b}}}_E^B \approx -\boldsymbol{\omega}^B \times \hat{\boldsymbol{b}}_E^B. \qquad (17)$$

Substituting the control torque (5) into (15) and using the fact that $\boldsymbol{a}^T(\boldsymbol{b} \times \boldsymbol{c}) = -\boldsymbol{b}^T(\boldsymbol{a} \times \boldsymbol{c})$, yields

$$\dot{V}(\boldsymbol{\omega}^B) = -(\boldsymbol{m}_c^B)^T(\boldsymbol{\omega}^B \times \boldsymbol{b}_E^B). \qquad (18)$$

Substituting (17) in (9) and assuming $\boldsymbol{m}_c^B = \boldsymbol{m}_d^B$ (ideal case), the time derivative of Lyapunov function yields

$$\dot{V}(\boldsymbol{\omega}^B) = -\left(\boldsymbol{\omega}^B \times \hat{\boldsymbol{b}}_E^B\right)^T k_{\dot{b}}(p)\left(\boldsymbol{\omega}^B \times \hat{\boldsymbol{b}}_E^B\right). \quad (19)$$

Despite the fact that $k_{\dot{b}}(p) > 0$ for all $p \in [0, 1]$, it is obvious from (19) that $\dot{V}$ is only negative semi-definite, i.e., $\dot{V} \le 0$. The kinetic energy associated with the component of $\boldsymbol{\omega}^B$ parallel to $\boldsymbol{b}_E^B$ (or equivalently to $\hat{\boldsymbol{b}}_E^B$) cannot be reduced. In other words, the control law (9) can effectively remove the satellite's angular momentum whenever $\boldsymbol{\omega}^B$ is not parallel to $\boldsymbol{b}_E^B$, while leaving it unchanged when $\boldsymbol{\omega}^T \boldsymbol{b}_E^B$ is zero [18]. This is due to the fact that the magnetorquers cannot provide torque along $\boldsymbol{b}_E^B$ as well as the magnetometer cannot sense this motion [7].

Thanks to the the orbital motion of the satellite, the Earth's magnetic field vector direction, $\hat{\boldsymbol{b}}_E^B$, does not remain fixed and global asymptotic stability (i.e., kinetic energy strictly decreasing) of the weighted B-dot controller can be proven by averaging-based analysis [18], by Lyapunov-like lemma derived from corollary to Barbalat's lemma [8], or by Krasovskii-LaSalle theory of periodic systems [2, 18].

Remark 2. *A natural design choice of* $\boldsymbol{\tau}_c^B$ *in* (15) *could be to generate torque according to*

$$\boldsymbol{\tau}_c^B = -k_\omega \boldsymbol{\omega}^B, \qquad k_\omega > 0. \qquad (20)$$

This choice ensures that (15) *is strictly negative, thus asymptotic stability guaranteed. However, a control law based on* (20) *would require angular rate measurements or its estimate. The latter can be accomplished by a*

computationally simple estimator based on magnetometer data only [19]. Unfortunately, (20) is not applicable in combination with pure magnetic actuation as the magnetorquers are only able to generate torques orthogonal to the Earth's magnetic field, see (5).

4. Discretised Algorithm

The weighted B-dot control law (9) needs to be implemented in the satellite's on-board computer as a discrete-time algorithm. In this section, the most important aspects of the on-board implementation are discussed.

4.1 Noise Filtering

One of the most cost-efficient way to filter out noise from the raw measurements (6) is to take the (weighted) average as follows

$$\tilde{\boldsymbol{b}}_E^B(t_k) = \sum_{i=1}^{n_s} w_i \left(\tilde{\boldsymbol{T}}_{S/B}^{(i)} \boldsymbol{z}_{raw}^{(i)}(t_k) + \tilde{\boldsymbol{b}}_{bias}^{(i)} \right), \quad (21)$$

where n_s is the total number of available sensors, $\tilde{\boldsymbol{b}}_E^B(t_k)$ is the filtered Earth's magnetic field in $\mathcal{F}_B$ at discrete time t_k, $w_i \geq 0$ are non-negative weights satisfying $w_1 + \ldots + w_{n_s} = 1$, $\tilde{\boldsymbol{T}}_{S/B}^{(i)} \in \mathbb{R}^{3 \times 3}$ is an estimate of the rotation matrix from the i-th sensor frame to $\mathcal{F}_B$, i.e., of $(\boldsymbol{T}_{B/S}^{(i)})^{-1}$, and $\tilde{\boldsymbol{b}}_{bias}^{(i)} \in \mathbb{R}^3$ is an estimate of the i-th sensor bias vector $\boldsymbol{b}_{bias}^{(i)}$. Both $\tilde{\boldsymbol{T}}_{S/B}^{(i)}$ and $\tilde{\boldsymbol{b}}_{bias}^{(i)}$ need to be estimated by an adequate calibration technique. The weights w_i can be used to reward or penalise measurements based on the accuracy of the respective sensor or fully disregard faulty sensors by setting the respective weight to zero. Ideally, sensors shall be placed apart to allow averaging out undesired magnetic fields generated by various on-board electronics.

4.2 Normalised B-dot Computation

If two consecutive measurements at t_{k-1} and t_k are available and the Nyquist criterion holds (see Section 4.5), then the normalised B-dot vector in (9) can be computed as

$$\dot{\hat{\boldsymbol{b}}}_E^B(t_k) = \frac{\hat{\boldsymbol{b}}_E^B(t_k) - \hat{\boldsymbol{b}}_E^B(t_{k-1})}{T_s}, \quad (22)$$

where $T_s \triangleq t_k - t_{k-1}$ is a constant sampling time between two consecutive measurements and $\hat{\boldsymbol{b}}_E^B(\cdot)$ is the normalised magnetic field computed as

$$\hat{\boldsymbol{b}}_E^B(\cdot) = \tilde{\boldsymbol{b}}_E^B(\cdot)/\|\tilde{\boldsymbol{b}}_E^B(\cdot)\|.$$

Clearly, both $\dot{\hat{\boldsymbol{b}}}_E^B$ and $\hat{\boldsymbol{b}}_E^B$ are estimates. The tilde symbol is left out above these vectors to simplify notation.

4.3 Tumble Parameter

To compute the scalar tumble parameter p for (9), we use the following discrete-time filter

$$p(t_k) = \frac{\alpha T_s}{2} \|\dot{\hat{\boldsymbol{b}}}_E^B(t_k)\| + (1 - \alpha)p(t_{k-1}), \quad (23)$$

where $\alpha > 0$ is the filter time-constant, $\dot{\hat{\boldsymbol{b}}}_E^B$ is computed as in (22), and the initial value of the filter, $p_0 \triangleq p(t_0)$, satisfies $0 \leq p_0 \leq 1$.

It is obvious from (22) and (23) that

$$0 \leq \|\dot{\hat{\boldsymbol{b}}}_E^B\| \leq 2/T_s \quad \Rightarrow \quad p \in [0, 1], \quad (24)$$

thus (23) satisfies the condition on p in (10). Thanks to the utilisation of the normalised B-dot vector in (23), the tumble parameter becomes altitude insensitive.

4.4 Discrete-time Controller

In this paper, we will assume constant currents for each axis. Only the current direction and duration will be controlled. Therefore, the absolute dipole moment achievable in any direction and per axis is

$$\bar{\boldsymbol{m}} \triangleq \begin{bmatrix} \bar{m}_x \\ \bar{m}_y \\ \bar{m}_z \end{bmatrix} = \begin{bmatrix} N_x A_x |i_x| \\ N_y A_y |i_y| \\ N_z A_z |i_z| \end{bmatrix}. \quad (25)$$

Once the desired magnetic dipole moment vector $\boldsymbol{m}_d^B \triangleq [m_{d;x}^B \ m_{d;y}^B \ m_{d;z}^B]^T$ is computed using (9), the amount of time each magnetorquer shall be activated is determined by

$$t_i^{on} = \delta T_s \min\left(1, \frac{|m_{d;i}^B|}{\bar{m}_i}\right), \quad i \in \{x, y, z\}, \quad (26)$$

where $t_i^{on} \geq 0$ is the "on-time" (duration) of the i-th magnetorquer and $0 < \delta < 1$ is the duty cycle of the magnetorquers within one control loop. To simplify implementation, we assume that one control cycle equals exactly to the duration of the measurement sampling time T_s.

The current direction in which the respective magnetorquer shall be activated is given by

$$d_i^{on} = m_i^{pol} \text{sign}\left(m_{d;i}^B\right), \quad i \in \{x, y, z\}, \quad (27)$$

where $d_i^{on} \in \{-1, 0, 1\}$ is the i-th magnetorquer's current direction and m_i^{pol} accounts for the winding polarity ($m_i^{pol} \in \{-1, 1\}$) or failure ($m_i^{pol} = 0$) of the i-th magnetorquer.

We assume that all the computations related to (26) and (27) are done with minimum delay and the magnetorquers are commanded immediately after that. The magnetorquers are switched off once the time they were supposed to be active has passed. The duty cycle δ shall be

selected carefully to allow enough time, $(1 - \delta)T_s$, for the magnetorquers to de-saturate and to account for the delayed control phenomenon. For the latter, see the discussion in the next subsection.

4.5 Sampling Time Selection

It is evident from (16) that the satellite's angular rate is directly linked with the change of the normalised vector of the Earth magnetic field in $\mathcal{F}_B$. From the Nyquist criterion [10], the maximum frequency of changes in the magnetic field that can be sensed without experiencing aliasing is $1/(2T_s)$. Therefore, the maximal rotational rate that can be measured from two consecutive measurements is π/T_s [rad/s], which yields to the following sampling time selection criterion

$$T_s \leq \frac{\pi}{|\omega_{max}|}, \tag{28}$$

where ω_{max} is the maximal expected rotational rate of the satellite in any axis and any direction.

From a control theory perspective, we need to carefully analyse the effect of the sampling time T_s and the duty cycle δ on the stability of the discretised B-dot control loop. In the subsequent analysis, we will follow similar steps as done in [17]. First, we will assume a rotation around the z-axis only, i.e., $\omega^B = [0 \ 0 \ \omega_z^B]^T$. In addition to that, we also assume the measurements being error-free, i.e., $\tilde{b}_E^B(\cdot) = b_E^B(\cdot)$, and that (17) is a valid approximation. Then, we can analytically expressed two consecutive magnetic field measurements as:

$$b_E^B(t_{k-1}) = \begin{bmatrix} b_{E;x}^B(t_{k-1}) \\ b_{E;y}^B(t_{k-1}) \\ b_{E;z}^B(t_{k-1}) \end{bmatrix},$$

$$b_E^B(t_k) = \begin{bmatrix} \cos(\omega_z^B T_s) & \sin(\omega_z^B T_s) & 0 \\ -\sin(\omega_z^B T_s) & \cos(\omega_z^B T_s) & 0 \\ 0 & 0 & 1 \end{bmatrix} b_E^B(t_{k-1}).$$

Subtracting the above two vectors yields

$$\Delta b_E^B(t_k) \triangleq b_E^B(t_k) - b_E^B(t_{k-1})$$
$$= \begin{bmatrix} \cos(\omega_z^B T_s) - 1 & \sin(\omega_z^B T_s) & 0 \\ -\sin(\omega_z^B T_s) & \cos(\omega_z^B T_s) - 1 & 0 \\ 0 & 0 & 0 \end{bmatrix} b_E^B(t_{k-1}).$$

It is clear that the above measurement vectors have the same magnitude, i.e., $\|b_E^B(t_k)\| = \|b_E^B(t_{k-1})\|$. Hence, the normalised B-dot vector can be expressed as

$$\dot{\hat{b}}_E^B(t_k) = \frac{1}{T_s} \frac{\Delta b_E^B(t_k)}{\|b_E^B(t_k)\|}. \tag{29}$$

The instantaneous torque at time $t = t_k$, generated by the desired magnetic dipole moment $m_d^B(t_k)$, is given by (32). By examining the last row, it is evident that in order the torque $\tau_{c;z}^B$ being opposite to the angular rate ω_z^B, $|\omega_z^B T_s|$ needs to be smaller than π. This leads again to the Nyquist criteria (28).

Suppose that the dipole moment $m_d^B(t_k)$ is applied for the entire duty cycle of the magnetorquers, i.e., during the interval $t \in [t_k, t_k + \delta T_s]$. By the end of this interval, the magnetic field in the body frame has changed to $b_E^B(t_k + \delta T_s)$ as well as the instantaneous torque generated by the magnetorquers changes to $\tau_c^B(t_k + \delta T_s)$. In order to reduce the rotation, the integral of the torque applied over the entire period $t \in [t_k, t_k + \delta T_s]$ should be negative. Suppose that $k_b(p)$ is constant during this interval, then for the z-axis, the negative torque condition becomes

$$\int_0^{\delta T_s} \tau_{c;z}^B(t)\mathrm{d}t = \kappa \int_0^{\delta T_s} [\sin(\omega_z t) - \sin(\omega_z(\delta T_s + t))]\,\mathrm{d}t$$
$$= 2\kappa \frac{\cos^2(\omega_z \delta T_s) - \cos(\omega_z \delta T_s)}{\omega_z} < 0, \tag{30}$$

where

$$\kappa = k_b(p) \frac{(b_x^B(t_{k-1}))^2 + (b_y^B(t_{k-1}))^2}{T_s\|b_E^B(t_k)\|^2} > 0.$$

Suppose that the z-axis is rotating at rate ω_{max}, i.e., $\omega_z = \omega_{max}$. Then, to satisfy the inequality (30), the sampling time T_s needs to satisfy the following condition

$$T_s < \frac{\pi}{2\delta|\omega_{max}|}. \tag{31}$$

$$\tau_c^B(t) = m_d^B(t_k) \times b_E^B(t) = -\frac{k_b(p)}{T_s\|b_E^B(t_k)\|^2} \Delta b_E^B(t_k) \times b_E^B(t)$$

$$= \frac{k_b(p)}{T_s\|b_E^B(t_k)\|^2} \begin{bmatrix} b_z^B(t_{k-1})\left(b_y^B(t_{k-1})(1 - \cos(\omega_z^B T_s)) + b_x^B(t_{k-1})\sin(\omega_z^B T_s)\right) \\ b_z^B(t_{k-1})\left(b_x^B(t_{k-1})(\cos(\omega_z^B T_s) - 1) + b_y^B(t_{k-1})\sin(\omega_z^B T_s)\right) \\ -\sin(\omega_z^B T_s)\left((b_x^B(t_{k-1}))^2 + (b_y^B(t_{k-1}))^2\right) \end{bmatrix}. \tag{32}$$

Note that the above process can be repeated for rotations around the remaining two axes.

To summarise the above analysis, in order to avoid aliasing and to be able to apply (on average) a torque in opposite direction to $\boldsymbol{\omega}^B$, the sampling time T_s shall be selected such that both conditions, (28) and (31), are simultaneously satisfied for the maximal expected rotation rate ω_{max}. For $\delta = 0.5$, the two conditions become equivalent. The negative torque criterion becomes a driving factor if $\delta > 0.5$.

4.6 Stopping Criterion and Tuning

To decide when the detumbling mode shall stop, one can use a simple threshold logic applied on the scalar tumble parameter p given by (23). However, in order to make sure that all axes have detumbled below a desired rate ω_{des}, we propose a vector version of (23) defined as follows

$$\boldsymbol{p}^v(t_k) = \frac{\alpha T_s}{2}|\dot{\hat{\boldsymbol{b}}}_E^B(t_k)| + (1-\alpha)\boldsymbol{p}^v(t_{k-1}), \quad (33)$$

where $\boldsymbol{p}^v \triangleq [p_x^v \ p_y^v \ p_z^v]^T$ is the vector-valued tumble parameter satisfying $\boldsymbol{p}^v(t_0) \triangleq \boldsymbol{p}_0^v$. The rest of the parameters are the same as in (23). Note that the absolute value $|\cdot|$ in (33) is applied element-wise.

The satellite is considered to be detumbled once the following inequality is satisfied (in all axes)

$$p_i^v(t) \le \bar{p}, \qquad \forall i \in \{x, y, z\}, \quad (34)$$

for a certain period of time $t \in [t_{k-N_w}, t_k]$, where $N_w \in \mathbb{N}$ is a confirmation window. N_w is introduced to enhance robustness. In (34), $\bar{p} > 0$ is a threshold parameter tuned such that the above inequality is met when the angular rate of the satellite is approximately ω_{des} in all axes. Care has to be taken when setting $\bar{p}$ in order not to exit the detumbling mode prematurely. Thanks to the use of the normalised B-dot in (33), the tuning of $\bar{p}$ becomes altitude independent.

The threshold logic (34) provides some hints for the variable control gain's (10) parameters selection. A large rate factor $\varphi \gg 1$ shall be chosen to penalise power consumption at the initial phase of the detumbling. If $\varphi < 1/\sqrt{3}\bar{p}$, then the parameter ε can be selected as $\varepsilon = 1 - \sqrt{3}\varphi\bar{p}$. This choice ensures that the B-dot gain is close to the sub-optimal value, i.e., $k_{\dot{p}}(p) \approx k_{\dot{p}}^*$, when the satellite is near to be detumbled.

5. Simulation Results for Delfi-PQ

In this section, we will demonstrated the performance of the proposed B-dot algorithm to detumble a fast-tumbling picosatellite. We consider the current picosatellite project of the Delft University of Technology, the Delfi-PQ project [1], as the baseline for our simulation study.

5.1 Simulation Parameters

We simulate a LEO and Sun synchronous Keplerian orbit and use the world geodetic system 1984 (WGS84) standard. The orbit-related parameters are given in Table 1. These orbital parameters imply an orbital period of approximately 1h and 32 min. The 12-th generation of the international geomagnetic reference field (IGRF) model was used to model the Earth's magnetic field vector in the body frame as

$$\boldsymbol{b}_E^B = \boldsymbol{T}_{IGRF/B}\boldsymbol{b}_E^{IGRF},$$

where $\boldsymbol{T}_{IGRF/B}$ is a rotation matrix from the IGRF to the body frame $\mathcal{F}_B$.

Table 1: Orbit-related parameters

Parameter	Value	Unit
Altitude	350	[km]
Eccentricity	0	[-]
Inclination	96.85	[deg]
RAAN	310	[deg]
Earth magnetic field	IGRF 12	[T]
Air density (low solar)	$2.01 \cdot 10^{-12}$	[kg·m^{-3}]

Table 2 gives an overview of the satellite-related parameters and their considered uncertainty ranges which were considered for the Monte Carlo (MC) simulations. The listed parameters represent realistic sensor and actuator characteristics. We consider two identical-type sensors being available on-board. Both sensors are corrupted with noises and suffer from unknown biases and quantization errors. For the magnetorquers, we model the effect of fall/rise times on the resulting magnetic dipole moment.

Table 2: Satellite-related parameters

Parameter	Nominal value	Unit	Uncertainty (1σ)
Mass	600	[g]	16.67%
Inertia principal moments $\{I_x, I_y, I_z\}$	$\{1.731,\ 1.726,\ 0.264\}$	[g·m^2]	21.67%*
Magnetorquer dipole moment**	0.002	[A·m^2]	15%
Residual dipole moment vector*** magnitude	0.0001	[A·m^2]	10%
Centre of pressure offset from CoM	$[5.4\ \ 2.0\ -8.2]$	[mm]	10%
Drag coefficient	2.1	[-]	N/A
Cross-sectional area {x, y, z} face	$\{92.1,\ 122.9,\ 25.2\}$	[cm^2]	N/A
Rise/fall times of the magnetorquers	0.01	[s]	N/A
Magnetometers' noise rms**	500	[nT]	N/A
Magnetometers' resolution**	300	[nT/LSb]	N/A
Magnetometers' bias vector*** magnitude	400	[nT]	N/A

* 16.67% due to the mass variations plus 5% individual uncertainty per axis; ** for all three axes;
*** direction uniformly distributed

The detumbling algorithm-related parameters are given in Table 3. The selected sampling time complies with both (28) and (31) criteria for our maximal expected angular rate of 180 [deg/s]. The threshold parameter $\bar{p}$ was tuned such that detumbling shall stop when $\omega_{des} \approx 5$ [deg/s] in all axes. The confirmation window N_w was selected to reflect a 30 minutes confirmation time. We assume that the magnetometers are not pre-calibrated, i.e., we do not account for the static biases which are present in the simulations.

Table 3: Detumbling algorithm-related parameters

Parameter	Value	Parameter	Value
T_s	0.25	$\boldsymbol{p}_0^v$	$[T_s\ \ T_s\ \ T_s]^T$
δ	0.6	$\bar{p}$	$8.1250 \cdot 10^{-3}$
α	1/200	$k_{\dot{b}}^*$	$1.2074 \cdot 10^{-6}$
φ	$4/T_s$	ε	$1 - \sqrt{3}\varphi\bar{p}$
p_0	$\sqrt{3}T_s$	N_w	$1800/T_s$
$w_1 = w_2$	1/2	$\tilde{\boldsymbol{b}}_{bias}^{(1)} = \tilde{\boldsymbol{b}}_{bias}^{(2)}$	$[0\ \ 0\ \ 0]^T$

For all simulations, the satellite is assumed to be detumbled (t_{ded}) when the condition given in (7) is satisfied for $\omega_{des} = 5$ [deg/s] (for all axes simultaneously). Where applicable, we also present the detumbling time estimated by the algorithm, see Section 4.6.

5.2 Sample Run Demonstration

Before turning to a statistical MC analysis, we present results from a sample run example. In this example, the satellite has nominal parameters and an initial rate of 180 [deg/s] in all three axes. The simulation runs for 16 orbits.

Figure 1 depicts the time behaviour of satellite's angular rates. It can be seen that the proposed algorithm is able to detumble a fast-tumbling picosatellite within less than a day. The algorithm confirmed detumbling with a delay of approximately half an hour. During the confirmation period, the satellite was still in active detumbling mode. Therefore, the angular rates around the detumbling confirmation are actually smaller than the desired rate ω_{des}.
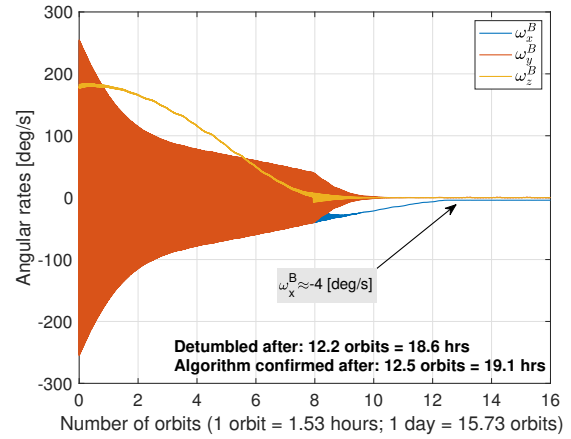

Figure 1: Satellite angular rate in body frame and detumbling performance from 180 [deg/s] in all three axes.

The weight that multiplies the sub-optimal B-dot gain, i.e., $k_{\dot{p}}(p)/k_{\dot{p}}^* = (\varphi p + \varepsilon)^{-1}$, and the scalar tumble parameter are depicted in Fig. 2. The measured magnetic field vector and the vector-valued tumble parameter together with the threshold parameter are shown in Fig. 3.
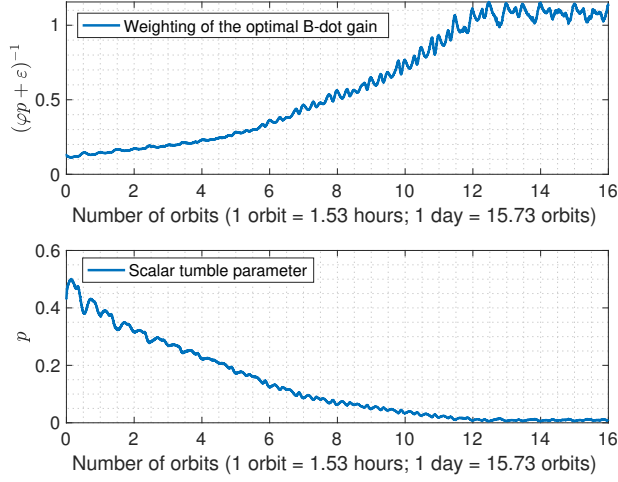
Figure 2: Sub-optimal B-dot gain weight (top) and scalar tumble parameter (bottom).
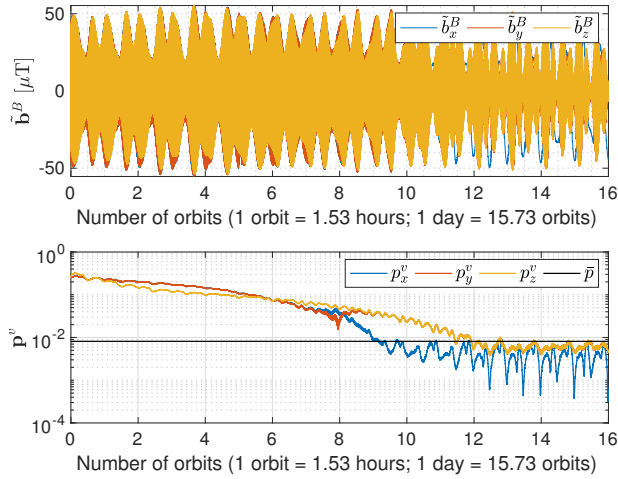

Figure 3: Measured magnetic field vector (top) and vector-valued tumble parameter (bottom, y-axis in log scale).

It is obvious from (25) and (26) that the magnetorquers power consumption is proportional to the amount of on-times. Hence, summing the magnetorquers on-times,

$$T^{on}_{tot;i} = \sum_{t_k=0}^{t_{det}} t^{on}_i(t_k), \qquad i \in \{x, y, z\},$$

can give us an indication about the power consumption of the algorithm. Figure 4 shows the commanded on-times per axis. The total opening time value, T^{on}_{tot}, is also shown for each axis.
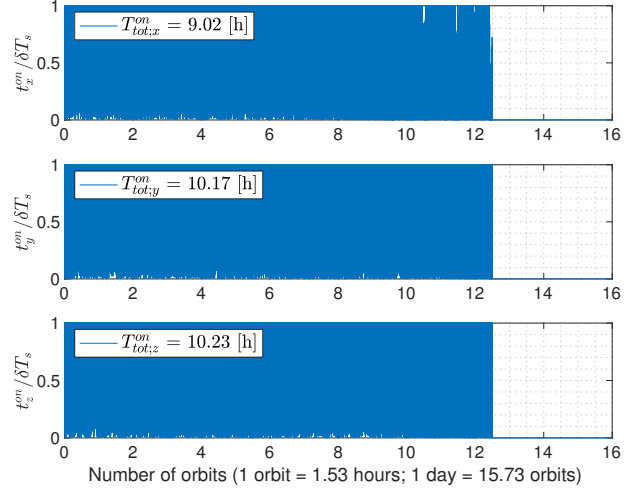

Figure 4: Normalised magnetorquer ON-times and sum of the opening ON-times until t_{det}.

5.3 Monte Carlo Analysis

In this subsection, we will present results based on 500 Monte Carlo simulation runs. For each run, we used different noise seeds and varied some satellite-related parameters according to the normal distribution and uncertainty characteristics given in Table 2. All simulations started with an initial angular rate of 180 [deg/s] in all three axes.

Table 4 shows the worst-case magnitudes estimate for various disturbance torques. It can be seen that the solar radiation pressure and gravity gradient disturbances have the lowest magnitude, hence they will not be considered for the MC analysis. Note that the considered atmospheric disturbance corresponds to a low solar activity scenario (air density: $\rho_{low} = 2.01 \cdot 10^{-12}$ [kg·m^{-3}]).

Table 4: Worst-case disturbance torque magnitudes

Disturbance	Magnitude [N·m]
Aerodynamic drag	$1.91 \cdot 10^{-8}$
Gravity gradient	$2.31 \cdot 10^{-9}$
Residual dipole	$5.03 \cdot 10^{-9}$
Solar radiation	$8.82 \cdot 10^{-10}$

Figure 5 depicts the histogram and a Gaussian fit of true detumbling times t_{det} obtained from the MC simulations. It can be observed, than on average, the proposed weighted B-dot law is able to detumble the satellites in less than 15 orbits.
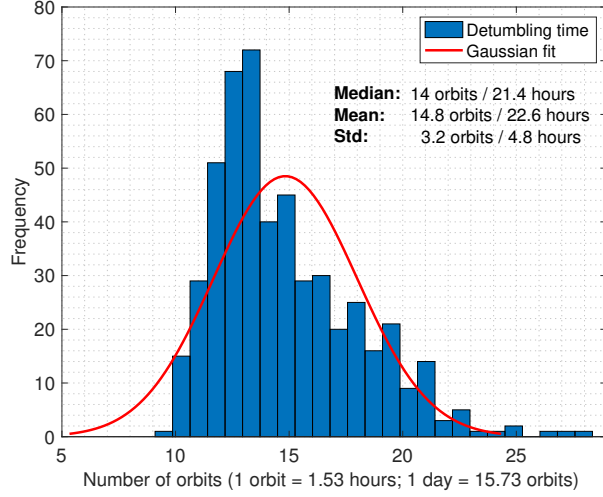
Figure 5: Histogram of the true detumbling time t_{det}.

Figure 6 depicts the detumbling time correlations with the principal moments of inertia and respective maximal dipole moments of the magnetorquers. As expected, there is a significant positive correlation with increasing mass moment of inertia, but relatively small negative correlation with the available dipole moment of the magnetorquers.
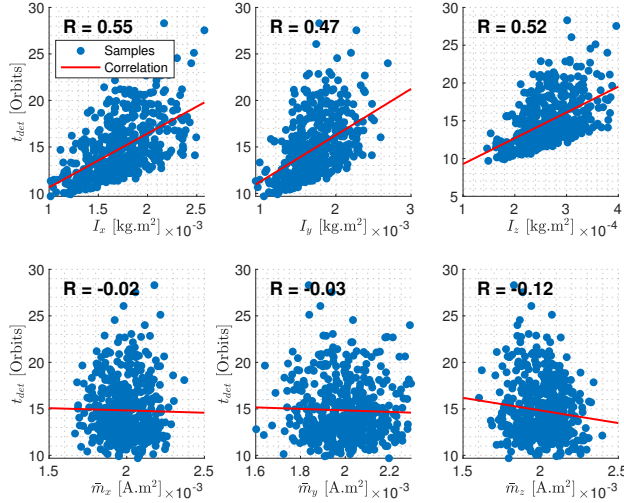

Figure 6: Detumbling time correlation with principal moments of inertia (top subplots) and with maximal dipole moments of the magnetorquers (bottom subplots).

In order to compare the proposed B-dot controller with the modified B-dot controller of Avanzini and Giulietti [8], we run additional 500 MC simulations for the same scenario as described above, but employing (9) with $k_{\dot{p}}(p) = k_{\dot{p}}^*$. The results are compared in Table 5. As can

be seen from this table, there is only a slight increase in the mean detumbling time, namely 0.45%, while the average power consumption of the magnetorquers is reduced noticeably.

Table 5: Detumbling performance comparison for $k_{\dot{p}}(p)$ and $k_{\dot{p}}^*$ from 180 [deg/s] (around all three axes). Results are given in hours.

Method/ Metric	Weighted B-dot		B-dot of [8]		
	μ	σ	μ	σ	η
t_{det}	22.63	4.83	22.52	4.85	0.45 %
$T_{tot;x}^{on}$	10.98	2.50	11.72	2.51	-6.32 %
$T_{tot;y}^{on}$	11.36	2.88	12.02	2.87	-5.43 %
$T_{tot;z}^{on}$	12.48	2.83	12.87	2.86	-3.05 %
$\sum_i T_{tot;i}^{on}$	34.82	7.17	36.61	7.72	-4.88 %

μ = mean; σ = standard deviation; η = relative mean error

To better appreciate the power consumption reduction, we have calculated the average sum of ON-times per orbit basis, denoted as $\mu(\boldsymbol{T}_{orb;i}^{on})$, where

$$\boldsymbol{T}_{orb;i}^{on} = \sum_{k \in \{orb\}} t_i^{on}(t_k), \qquad i \in \{x, y, z\}$$

The values of $\mu(\boldsymbol{T}_{orb;i}^{on})$ for each axis are compared in Figure 7 for the two considered B-dot laws. A reduction in average power consumption can be observed (especially at the beginning of the detumbling) for the weighted B-dot controller. It shall be noted that no tuning has been performed to optimise φ and ε for power efficiency or detumbling time.
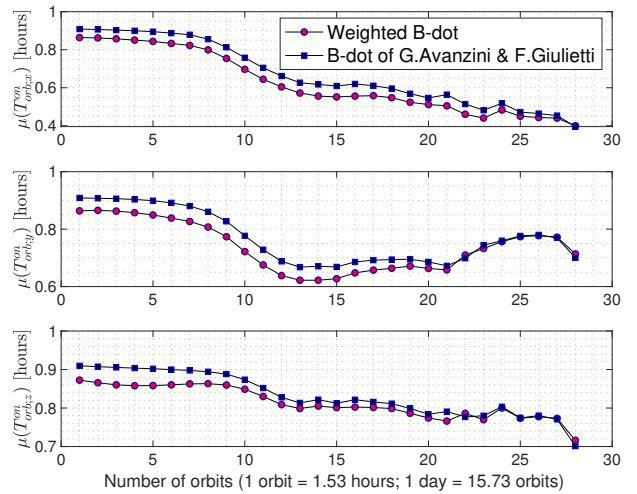

Figure 7: Comparison of the average on-times per orbit basis.

6. Conclusions

The problem of pure magnetic detumbling of a fast-tumbling picosatellite was studied. A new weighted B-dot controller has been proposed. This controller enables power consumption reduction while not significantly increasing the time it takes to detumble. Monte Carlo simulation results have revealed that it is possible to save almost 5% of power while sacrificing only about 0.5% of the detumbling performance when compared to the same control strategy with constant control gain.

Acknowledgements

The authors would like to thank the members of the Delfi-PQ team for their helpful discussions on practical aspects of the detumbling algorithm implementation.

References

[1] S. Radu, M. S. Uludağ, S. Speretta, J. Bouwmeester, E. Gill, and N. Chronas Foteinakis. Delfi-PQ: The First Pocketqube of Delft University of Technology. In *International Astronautical Congress*, 2018. IAC-18-B4.6B.5.

[2] R. Wisniewski. *Satellite attitude control using only electromagnetic actuation*. PhD thesis, Aalborg University, December 1996.

[3] J. T. Gravdahl. Magnetic attitude control for satellites. In *Conference on Decision and Control*, volume 1, pages 261–266. IEEE, 2004.

[4] C.D. Maclean, D. Pagnozzi, and J. Biggs. Computationally light attitude controls for resource limited nano-spacecraft. In *International Astronautical Congress*, 2011. Paper IAC–11-C1.6.8.

[5] M. Yu. Ovchinnikov, D.S. Roldugin, and V.I. Penkov. Three-axis active magnetic attitude control asymptotical study. *Acta Astronautica*, 110:279–286, 2015.

[6] D. Baldacchino, D Debattista, R Rotin, D. Cachia, M. A. Azzopardi, S. G. Fabri, and M. K. Bugeja. Review and Feasibility of Active Attitude Control and Detumbling for the UoMBSat-1 PocketQube Pico-Satellite. In *Mediterranean Conference on Control and Automation*, pages 1237–1243. IEEE, 2017.

[7] A.C. Stickler and K. T Alfriend. Elementary magnetic attitude control system. *Journal of Spacecraft and Rockets*, 13(5):282–287, 1976.

[8] G. Avanzini and F. Giulietti. Magnetic detumbling of a rigid spacecraft. *Journal of Guidance, Control, and Dynamics*, 35(4):1326–1334, 2012. doi: 10.2514/1.53074.

[9] M. J. Sidi. *Spacecraft dynamics and control: a practical engineering approach*, volume 7. Cambridge University Press, 2000.

[10] J. R. Wertz. *Spacecraft attitude determination and control*, volume 73. Springer Science & Business Media, 2012.

[11] L.J. Kamm. Magnetorquer-a satellite orientation device. *ARS Journal*, 31(6):813–815, 1961.

[12] J. Li, M. Post, T. Wright, and R. Lee. Design of attitude control systems for cubesat-class nanosatellite. *Journal of Control Science and Engineering*, 2013: 4, 2013.

[13] F.L. Markley. Attitude control algorithms for the solar maximum mission. In *Guidance and Control Conference*, pages 59–69. AIAA, August 1978.

[14] J. Reijneveld and D. Choukroun. Attitude control system of the Delfi-n3Xt satellite. *Progress in Flight Dynamics, GNC, and Avionics*, 6:189–208, 2013.

[15] M. Yu Ovchinnikov, D.S. Roldugin, S.S. Tkachev, and V.I. Penkov. B-dot algorithm steady-state motion performance. *Acta Astronautica*, 146:66–72, 2018.

[16] H.C. Chang, W.L. Chiang, and Y.Y. Lian. Efficiency investigation of conventional satellite initial acquisition control with the consideration of orbital motion. *Procedia Engineering*, 67:128–139, 2013.

[17] P. Reijneveld. Design of the Attitude Determination and Control Algorithms for the Delfi-n3Xt. Master's thesis, Delft University of Technology, January 2012.

[18] M. Lovera. Magnetic satellite detumbling: The b-dot algorithm revisited. In *American Control Conference*, pages 1867–1872. IEEE, 2015.

[19] P. Tortora, Y. Oshman, and F. Santono. Spacecraft angular rate estimation from magnetometer data only using an analytic predictor. *Journal of Guidance, Control, and Dynamics*, 27(3):365–373, 2004.